2013 IEEE 10th International Symposium on Biomedical Imaging:
From Nano to Macro
San Francisco, CA, USA, April 7-11, 2013

IMPROVED VISUALIZATION AND QUANTIFICATION OF 4D FLOW MRI DATA USING DIVERGENCE-FREE WAVELET DENOISING

F Ong[1]*, M Uecker*[1]*, U Tariq*[2]*, A Hsiao*[2]*, MT Alley*[2]*, SS Vasanawala*[2] *and M Lustig*[1]

[1]Electrical Engineering and Computer Sciences, University of California, Berkeley
[2]Radiology, Stanford University

ABSTRACT

4D flow MRI is a promising method for providing global quantification of cardiac flow in a single acquisition, yet its use in clinical application suffers from low velocity-to-noise ratio. In this work, we present a novel noise reduction processing for 4D flow MRI data using divergence-free wavelet transform. Divergence-free wavelets have the advantage of enforcing soft divergence-free conditions when discretization and partial voluming result in numerical non-divergence-free components and at the same time, provide sparse representation of flow in a generally divergence-free field. Efficient denoising is achieved by appropriate shrinkage of divergence-free and non-divergence-free wavelet coefficients. To verify its performance, divergence-free wavelet denoising was performed on simulated flow and compared with existing methods. The proposed processing was also applied on *in vivo* data and was demonstrated to improve visualization of flow data while preserving quantifications of flow data.

Index Terms— 4D flow MRI, divergence-free, wavelets, denoising, visualization

1. INTRODUCTION

Time-resolved 3D phase-contrast MRI (4D flow MRI) has the potential to provide both anatomy and function of cardiac flow globally in a single acquisition [1]. However, 4D flow data are often compromised by low velocity-to-noise ratio, potentially caused by MRI accelerated acquisitions or high velocity encodes (high vencs). These methods are oftentimes neccesary to provide practical scan time and to avoid velocity aliasing when the dynamic range of velocites is high. To reduce noise level, physical properties of blood flow can be exploited to identify important features and separate the noise from the flow data. Since blood flow is incompressible, it is approximately divergence-free. Therefore, most of the divergence components in the flow field originate from either noise or artifacts, which can be reduced by enforcing the flow to be divergence-free. However, in practice, discrete approximation and partial voluming of flow cannot be fully captured by strict divergence-free representation. This situation often occurs in places near edges of flow, static tissue or turbulent flow. Strict divergence-free enforcement across boundaries may result in significant error propagation throughout the flow field. Hence, we assert that a practical and effective divergence-free enforcing processing of flow data should have all of the following properties:

1. It should enforce appropriate divergence-free constraints on different parts of the flow data.
2. It should have multiscale enforcement of divergence-free constraints.
3. It should be adaptive to noise.
4. It should be computationally fast.

In this current paper, we present and analyze a noise reduction processing that accomplishes the above goals by using divergence-free wavelet transform. In addition, we show that divergence-free wavelets provide a sparse representation of flow data, which we utilized for further denoising by performing wavelet shrinkage [2].

2. BRIEF REVIEW OF PREVIOUS WORKS

Among previous works, Song *et al.* [3] solved for a divergence-free field using finite difference method (FDM), which was partly solved by a fast sine transform, while Busch *et al.* [4] constructed a divergence-free field by projecting the noisy flow field onto divergence-free radial basis functions (RBF) using iterative least squares. Both were shown to be effective as a denoising process [5]. However, both methods enforce the flow field to be strictly divergence-free and require accurate segmentation to prevent unwanted divergence-free enforcing near edges. This could result in error propagation in response to errors near boundaries.

3. APPROACH

3.1. Wavelet Denoising

Signal denoising through wavelet shrinkage was popularized by Donoho and Johnstone [2] in the 90s and is now widely used in many imaging applications. The popularity of wavelet denoising is encouraged by many attractive properties

This work is supported in part by NIH grant R01EB009690, American Heart Association 12BGIA9660006, Hellman Family fund and Intel SRC

of wavelet methods, such as efficient multiscale decompositions, edge preserving transforms, and sparse representation of signals, while accounting to only $O(N)$ complexity, where N is the data size. These appealing features of wavelet denoising motivate us to find a suitable wavelet domain for similar processing on 4D flow data.

3.2. Divergence-free Wavelets

Like many scientific and engineering fields, the computational fluid dynamics (CFD) community was significantly impacted by the introduction of wavelets in the late 1980s. In particular, Lemarie-Rieusset [6] designed compactly supported divergence-free wavelets, which have been investigated in several CFD applications. Among these applications, divergence-free wavelet was shown to provide a sparse representation for simulated flow data in [7] and was demonstrated to have the capability of separating statistically random flow in [8]. These two properties encourage us to apply divergence-free wavelet denoising in the context of flow MRI.

Despite the name of divergence-free wavelet transform, 3D divergence-free wavelets span the entire set of 3D vector fields and separate flow data into divergence-free and non-divergence-free components. Thus, to effectively denoise flow data, we propose soft-thresholding divergence-free wavelet coefficients to encourage sparsity; in addition, we soft-threshold non-divergence-free wavelet coefficients with a higher threshold to softly enforce divergence-free constraints instead of eliminating all divergence. Soft-thresholding non-divergence-free coefficients allows the flexibility to adjust the cutoff so that important non-divergence-free components, such as those arising near edges, persist. Hence, this operation does not enforce strict divergence-free constraints across edges and is more tolerable to errors near boundaries.

The construction of divergence-free wavelets relies on the following proposition that relates two different wavelets by differentiation [7]:

Proposition: Let $\phi_1(x)$ and $\psi_1(x)$ be a 1D derivable scaling function and wavelet function respectively. Then we can build another 1D scaling function $\phi_0(x)$ and wavelet function $\psi_0(x)$ such that

$$\phi_1{}'(x) = \phi_0(x) - \phi_0(x-1) \qquad \psi_1{}'(x) = 4\psi_0(x)$$

As noted in [8], for compactly supported wavelets, only biorthogonal 1D wavelets can satisfy the proposition, which implies that eliminating non-divergence-free components is not an orthogonal projection onto the space of divergence-free vector fields. However, if we choose appropriate wavelets, such as spline wavelets, which are known for its near-orthogonality, then divergence-free wavelets are close to orthogonal as shown in [8].

Using the above proposition, divergence-free wavelets can then be explicitly constructed by combining tensor products of these functions. For example, a 2D divergence-free scaling and wavelet function can be of the form:

$$\Phi_{divfree}(x,y) = \begin{pmatrix} \phi_1(x)[\phi_0(y) - \phi_0(y-1)] \\ -[\phi_0(x) - \phi_0(x-1)]\phi_1(y) \end{pmatrix}$$

$$\Psi_{divfree}(x,y) = \begin{pmatrix} \psi_1(x)\psi_0(y) \\ -\psi_0(x)\psi_1(y) \end{pmatrix}$$

which can be verified to have zero divergence. Similar procedure can be extended to the case of three-dimensional and used to generate a complete set of 21 divergence-free wavelet functions following the instructions in [7]. Some examples of divergence-free wavelet basis functions are shown in Fig. 1.

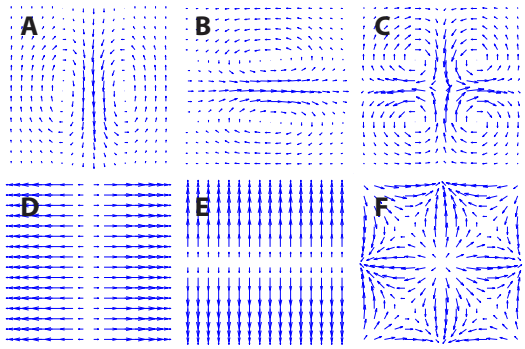

Fig. 1: *Examples of 2D slices of divergence-free wavelet basis functions: divergence-free* ***(A,B,C)*** *and non-divergence-free* ***(D,E,F)***

More importantly, tensor combination of 1D wavelet functions implies that computation of divergence-free wavelet coefficients is reduced to a simple linear combination of wavelet coefficients generated by standard 3D wavelet transform using ϕ_0, ψ_0, ϕ_1 and ψ_1. Thus, the procedure of divergence-free wavelet denoising is only different from standard 3D wavelet transforms in that we have to linearly combine wavelet coefficients before and after soft-thresholding and maintains $O(N)$ complexity as illustrated in Fig. 2.

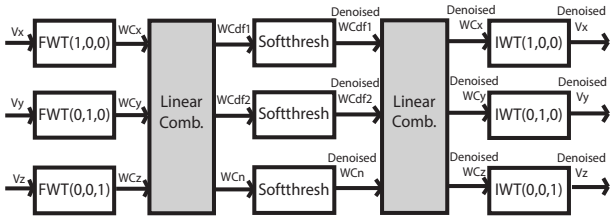

Fig. 2: *Flow diagram of divergence-free wavelet denoising. [FWT:Forward Wavelet Transform, IWT:Inverse Wavelet Transform, WC:Wavelet Coefficient, df:divergence-free, n:non-divergence-free, (a,b,c):*($\{\phi_a(x), \psi_a(x)\}$, $\{\phi_b(x), \psi_b(y)\}$, $\{\phi_c(x), \psi_c(z)\}$)*]*

4. RESULTS AND DISCUSSION

To validate the performance of divergence-free wavelet denoising, the processing was tested on simulated flow data and *in-vivo* 4D flow data. Divergence-free wavelet denoising was implemented in Matlab (The MathWorks, Natick, MA, USA) on a Intel Core 2 Duo laptop with 4GB of RAM, following the instructions in [7]. Linear spline wavelet (Cohen-Daubechies-Feauveau 2.2) was used for ϕ_0 and ψ_0, and quadratic spline

wavelet (Cohen-Daubechies-Feauveau 3.1) was used for ϕ_1 and ψ_1. Thresholds were chosen to balance visualization and data consistency. Non-divergence-free threshold was set to be roughly twice the divergence-free threshold.

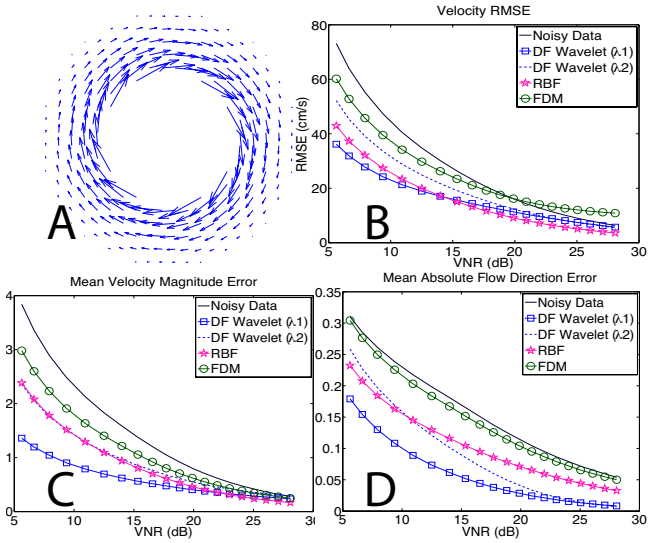

Fig. 3: *(in color) Calculated Couette velocity field* ***(A)****. Velocity RMSE (cm/s) v. VNR* ***(B)****. Mean velocity magnitude error (unitless) v. VNR* ***(C)****. Mean absolute flow direction error (from 0 to 1) v. VNR* ***(D)****. [λ_1: Thresholds fixed at 4σ and 7σ for div-free and non-div-free coefficients. λ_2: Thresholds fixed at 7σ for all coefficients]*

4.1. Simulation

For our simulation, we constructed a 32^3 Couette flow field (shown in Fig. 3), which had the form:

$$v_x = -(Ar + B/r)sin\theta, \quad v_y = (Ar + B/r)cos\theta, \quad v_z = 0$$

where $r = \sqrt{x^2 + y^2}, \theta = tan^{-1}(y/x)$ and A and B are constants such that maximum speed is 300 cm/s. We simulated complex data acquired with a 5-point balanced phase-contrast method and assumed fully-sampled Fourier transform reconstruction. The complex data magnitude in image domain was set to one where velocity field was nonzero and zero otherwise, while the complex signal phase was constructed by adding or subtracting velocity components according to the 5-point balanced phase-contrast method, with the constant phase assumed to be zero. Different levels of complex Gaussian noise with variance σ^2 were added to the complex data. Divergence-free wavelet denoising was applied on the flow data extracted from phase and was compared with existing methods using FDM and RBF, following the instructions in [3, 4]. For divergence-free wavelet denoising, we considered two cases of thresholding: (λ_1) Thresholds fixed at 4σ and 7σ for divergence-free and non-divergence-free coefficients, and (λ_2) thresholds fixed at 7σ for all coefficients. For RBF, the size of basis functions was set to be 7^3. Image magnitude was used to remove phase in zero magnitude regions for all methods. Velocity-to-noise ratios (VNR) and mean errors were estimated by averaging over 50 experiments and over voxels with nonzero image magnitude. We defined velocity magnitude error and absolute flow direction error for each voxel as:

$$\frac{\|v_{calc}\| - \|v_{processed}\|}{\|v_{calc}\|} \quad , \quad 1 - \frac{|v_{calc} \cdot v_{processed}|}{\|v_{calc}\|\|v_{processed}\|}$$

Displayed in Fig. 3, the results showed that the proposed divergence-free wavelet denoising (λ_1) performed better than other methods in velocity magnitude error and absolute flow direction error, while achieving low root-mean-square-error (RMSE), second only to RBF in high VNR. We also note that divergence-free wavelet denoising with threshold (λ_1) performed better than threshold (λ_2).

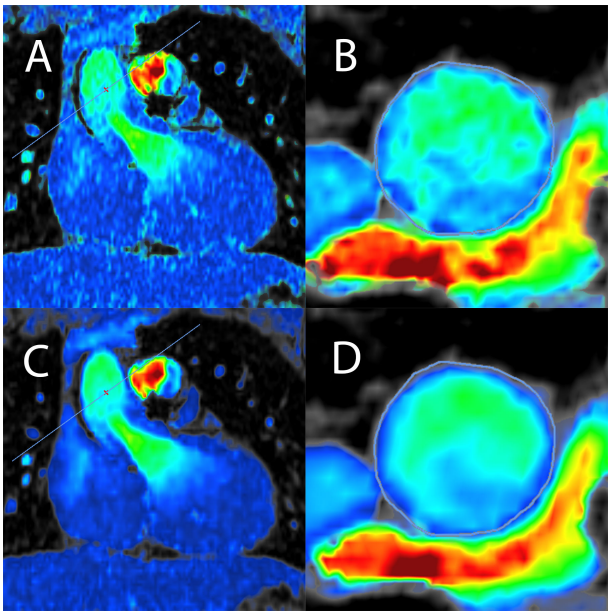

Fig. 4: *(in color) Visualization of cardiac flow magnitudes before denoising* ***(A)*** *with closeup of segmented aorta slice* ***(B)****, and after denoising* ***(C)*** *with closeup of segmented aorta slice* ***(D)****.*

4.2. *In-vivo* flow data

Divergence-free wavelet denoising was further tested on *in-vivo* data. *In-vivo* 4D cardiac flow data were acquired in 8 patients with 20 cardiac phases, 122-144 slices and an average spatial resolution of 1.56x1.56x1.43mm^3 on a 1.5T GE Signa Scanner. The acquisition was undersampled by 4 to achieve practical scan time and was reconstructed using L1-SPIRiT, a compressed sensing and parallel imaging reconstruction [9]. Flow data were extracted from eddy-current corrected phase of reconstructed images. Segmentations were done manually on aorta and pulmonary trunk. Net flow rate(volume/time) and regurgitant fraction(%) were calculated for each segmentation. Since the net flow difference between aorta and pulmonary trunk should generally be zero, we defined flow inconsistency as the absolute difference between flow rates in

the aorta and pulmonary trunk. Divergence-free wavelet denoising was applied on 3D volumes for each cardiac phase. The computation for each phase took less than half a minute using a Matlab implementation.

Studies were evenly separated into a group with regurgitant fractions less than 5% (mean net flow=2.945 L/min) and a group with regurgitant fractions more than 30% (mean net flow=2.212 L/min). For the first group, the average flow inconsistency before denoising was 0.395 L/min and after denoising was 0.353 L/min, yielding a 10.7% improvement. Average change in regurgitant fraction was 0.08%. For the second group, the average flow inconsistency before denoising was 1.151 L/min and after denoising was 0.926 L/min, yielding a 19.5% improvement. Average change in regurgitant fraction was 1.88%. Here, we emphasize that the change in regurgitant fraction for both groups was small, which suggests that divergence-free wavelet denoising can be safely applied on clinical data while improving visualization (Fig. 4).

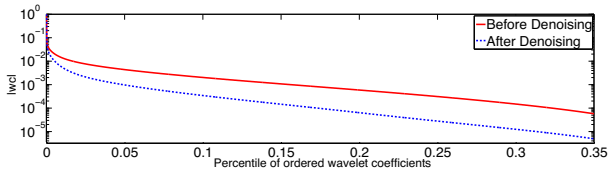

Fig. 5*: Normalized absolute value of wavelet coefficients with respect to largest coefficient v. percentile of ordered wavelet coefficients of a* in-vivo *dataset*

Analyzing *in-vivo* datasets, we demonstrated the sparsity of flow data in divergence-free wavelet domain in Fig. 5, in which we plotted normalized absolute value of wavelet coefficients with respect to the largest coefficient versus percentile of ordered wavelet coefficients (0 being the largest wavelet coefficient and 1 being the smallest wavelet coefficient). We observed that even for the noisy acquired data, more than 97% of wavelet coefficients were smaller than 1% of the largest wavelet coefficient. In addition, in Fig. 6, we showed the effect of applying thresholds on non-divergence-free wavelet coefficients. Notice that the non-divergence-free coefficients near edges were largely intact and hence did not enforce divergence-free constraints across edges.

5. CONCLUSION

Divergence-free wavelet denoising was shown to enhance the visual quality of 4D flow data and improve quantification of flow at aorta and pulmonary trunk. The processing was shown to be comparable to other processing on simulated data while providing computational efficiency and tolerance to boundary errors. Divergence-free wavelet transform was also demonstrated to provide a sparse transformation for 4D flow data.

6. REFERENCES

[1] M. Markl, F. P. Chan, M. T. Alley, K. L. Wedding, M. T. Draney, C. J. Elkins, D. W. Parker, R. Wicker, C. A. Taylor, R. J. Herfkens, and N J. Pelc, "Time-resolved three-dimensional phase-contrast MRI.," *J Magn Reson Imaging*, vol. 17, no. 4, pp. 499–506, 4 2003.

[2] D. L. Donoho and J. M. Johnstone, "Ideal spatial adaptation by wavelet shrinkage," *Biometrika*, vol. 81, no. 3, pp. 425–455, 1994.

[3] S. M. Song, S. Napel, G. H. Glover, and N. J. Pelc, "Noise reduction in three-dimensional phase-contrast mr velocity measurementsl," *Journal of Magnetic Resonance Imaging*, vol. 3, no. 4, pp. 587–596, 1993.

[4] J. Busch, D. Giese, L. Wissmann, and S. Kozerke, "Construction of divergence-free velocity fields from cine 3d phase-contrast flow measurements.," *Magn Reson Med*, 3 2012; doi: 10.1002/mrm.24221.

[5] M. Leocher, S. Kecskemeti, K. Johnson, P. Turski, and O. Wieben, "Evaluation of divergence-free correction algorithms in high resolution 4-d flow images of cranial vasculature.," in *Procs. of the ISMRM*, 2012, p. 1246.

[6] P. G. Lemarié-Rieusset, "Analyses multi-résolutions non orthogonales, commutation entre projecteurs et derivation et ondelettes vecteurs à divergence nulle," *Revista Matemática Iberoamericana*, vol. 8, no. 2, pp. 221–238, 1992.

[7] E. Deriaz and V. Perrier, "Towards a divergence-free wavelet method for the simulation of 2d/3d turbulent flows," *J. Turbul*, vol. 1, 2006.

[8] E. Deriaz, M. O. Domingues, V. Perrier, K. Schneider, and M. Farge, "Divergence-free wavelets for coherent vortex extraction in 3d homogeneous isotropic turbulence," in *ESAIM: Proceedings*, 2007, vol. 16, pp. 146–163.

[9] M. Lustig and J. M. Pauly, "Spirit: Iterative self-consistent parallel imaging reconstruction from arbitrary k-space," *Magnetic Resonance in Medicine*, vol. 64, no. 2, pp. 457–471, 2010.

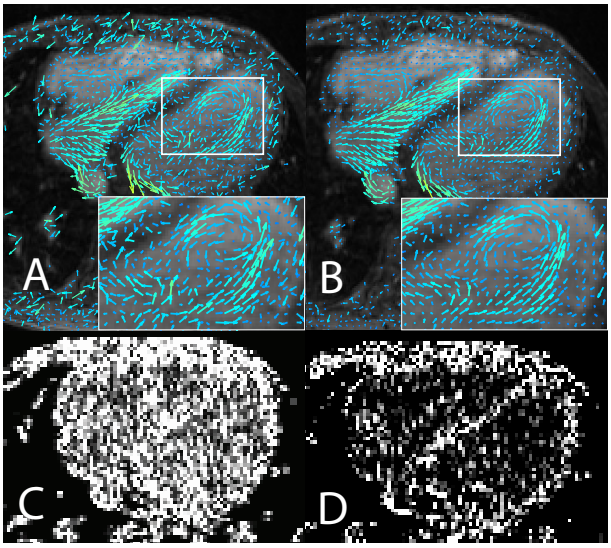

Fig. 6*: (in color) Vector visualization of axial cross-section of cardiac flow: Acquired data* ***(A)****, Denoised data* ***(B)****. Corresponding wavelet coefficients: Acquired data* ***(C)****, Denoised data* ***(D)****.*